HIGH FIELD MRI OF HYDRATE PHASE TRANSITIONS IN SANDSTONE

S. Almenningen[1], J. Gauteplass[2], V.F. Veland[1], G.L. Aastveit[3], P. Fotland[3], and G. Ersland[1]
[1]Department of Physics and Technology, University of Bergen, Norway
[2]Department of Chemistry, University of Bergen, Norway
[3]Statoil ASA, Bergen, Norway

This paper was prepared for presentation at the International Symposium of the Society of Core Analysts held in Trondheim, Norway, 27-30 August 2018.

ABSTRACT

This paper reports a methodology for high field magnetic resonance imaging (MRI) and nuclear magnetic resonance (NMR) T_2 spectroscopy of hydrate-bearing porous media. We used a 4.7 Tesla MR-scanner with connected high-pressure and high-precision pumps to facilitate direct visualization of gas hydrate phase transitions in sediments. Experiments were designed to measure the correlation between water saturation in Bentheimer sandstone cores and obtained MR signal intensity. Gas hydrates were formed from 65% of the pore volume occupied by water (0.1 wt% NaCl) and 35% by gas (78% methane and 22% propane). The specific gas mixture was chosen to provide hydrate stable conditions at room temperature (21°C) and moderate pressures (above 5 MPa). Both hydrate formation and dissociation events were initiated and monitored by pore pressure control. Two types of MR pulse sequences are reported: (1) RAREst, used to image and analyze the spatial development in the pore volume of the core, and (2) CPMG to map T_2 relaxation changes during hydrate growth and dissociation. Phase transitions of gas hydrate in Bentheimer sandstone cores were successfully imaged by high field MRI, and benefits from reduced measuring time and enhanced spatial resolution compared with experiments using lower field strengths. Obtained T_2 distributions during hydrate formation indicate pore-filling hydrate growth in the largest pores.

INTRODUCTION

Gas hydrates are clathrates composed of hydrogen-bonded water molecules encapsulating one or more guest molecules. Typical examples of guest molecules are methane, propane, and carbon dioxide (CO_2). Natural gas hydrates form at locations where water and gas are present under moderate-to-high pressures and low temperatures, e.g. in deep-sea continental shelves or in permafrost regions. There is an abundance of natural gas hydrate reservoirs around the world, and estimates of the total amount of methane gas trapped in hydrates range between 10^{14} - 10^{18} Sm^3 [1]. Consequently, field pilots are tested worldwide as an effort toward full-scale development of gas hydrates as an energy resource [2-4]. Injection of anthropogenic CO_2 into natural hydrate reservoirs lead to spontaneous exchange of guest molecules in the hydrate-bearing sediment layers.

This concept combines permanent CO_2 storage with natural gas production in a carbon-neutral production strategy [5]. Hydrate agglomerates tend to block the pore space and impede rock permeability under favorable thermodynamic conditions. This sealing property of hydrates can provide for a naturally developing secondary gas seal and prevent upward gas migration in CO_2 storage schemes [6]. To realize hydrates as a vast energy source or as a trapping mechanism in carbon sequestration, in-depth knowledge of hydrate formation and dissociation kinetics in sediments are called for.

Non-invasive imaging of gas hydrate studies in laboratory opaque systems has proven successful for hydrate formation, dissociation, and distribution. Imaging techniques are categorized into 1) attenuation methods and 2) explicit methods. Attenuation methods (e.g. computed tomography, CT) measure the gradual loss in X-ray flux intensity through the medium, and produce a time-averaged density distribution image of the rock [7]. Spatial fluid saturation is derived with sufficient fluid density difference. Explicit methods (e.g. magnetic resonance imaging, MRI) detect the fluid directly, independent of the porous media [8, 9]. MRI is a precise imaging tool and maps liquid water protons in three dimensions within the field of view. Signal from hydrogens in solids, e.g. hydrate crystals and ice, are not acquired due to their much shorter relaxation time. Conversion of liquid water to solid constituent of the hydrate structure is manifested as a loss of signal intensity, and makes MRI an effective technique to distinguish between the hydrate product and initial host- and guest molecules [10].

MRI has mainly been used in gas hydrate research at low and intermediate magnetic field strengths [5, 11-14], and occasionally at higher magnetic field strength [15]. High field and ultra-high field MRI benefits from enhanced sensitivity compared with lower field strengths; shorter measuring time, and improved spatial resolution and signal-to-noise-ratio are reported in clinical studies [16-18]. In this high field MRI study, we cover two important aspects related to gas hydrate research: 1) correlate the mean signal intensity to water saturation in sediments from different MRI settings, and 2) apply the correlation to quantify hydrate phase saturation and distribution in sandstone core samples.

EXPERIMENTAL PROCEDURE

Cylindrical Bentheimer sandstone cores are used as host sediment for the hydrate phase transitions. The average porosity and permeability is 23% and 1.1 D, respectively. The specialized core holder is made from PEEK and titanium materials to ensure compatibility with the MR instrument (Figure 1). Floating end-pieces on each side of the core are positioned inside the rubber sleeve providing uniaxial core confinement by pressurized fluorinert (containing no hydrogen). Both flow lines leading into the core are connected to a high-pressure, high-precision pump. The entire core holder containing core material surrounded by confinement fluid is placed inside the MR instrument for real time image acquisition. The superconductive magnet (BioSpec series provided by Bruker) has a magnetic field strength of 4.7 T (200 MHz) and can accommodate cylindrical core holders with diameters up to 19 cm. The longitudinal field of view is

limited to 12 cm. The pore pressure is controlled by the high-pressure pump and all experiments are conducted at room temperature (21°C).

Calibration Study
Initial calibration tests of partially water-saturated cores were conducted to evaluate the applicability of using image intensity calculations obtained from MRI to quantify water saturation. A total of eight different Bentheimer sandstone cores (length and diameter of 15 cm and 4.8 cm, respectively) were saturated with air and water containing 0.1 wt% sodium chloride (NaCl). The water saturation ranged from 27 to 68%, and the cores were subsequently imaged with the 2D scan protocol RAREst (=Rapid Acquisition with Relaxation Enhancement with short echo time). This scan provided short echo times (echo time = 5.66 ms, rare factor = 2) and fast acquisition (scan time = 10.5 min). Ten axial slices with dimensions 60x60x10 mm were positioned uniformly throughout the length of the core, and the voxel resolution was set to 0.5x0.5x10 mm. Each slice was circularly cropped during post-processing to map the cross-sectional area of the core. The average voxel intensity for the whole core was then calculated as the arithmetic mean of every voxel in every slice. The background noise was limited during scans but corrections were routinely implemented.

Hydrate Study
The Bentheimer sandstone specimen used in the hydrate study had length equal to 10.0 cm and diameter of 3.81 cm. The pore space was initially saturated with 65% water containing 0.1 wt% NaCl. A mixture of 22% propane and 78% methane was used as hydrate former to enable hydrate growth at room temperature (21°C). The hydrate forming pressure at 21°C is 5.3 MPa when the salt content is 0.1 wt% NaCl [19]. The gas mixture was introduced to the core sample from the high-pressure pump and the pore pressure was increased to 10.0 MPa while continuously keeping the confinement pressure 3.0 MPa higher. Hydrate formation was monitored by constant pressure operation of the pump (mass balance) and by continuous image acquisition. The scan protocol RAREst (echo time = 4.8 ms, rare factor = 2) was used for visualization and CPMG scans (400 echoes with spacing = 5.0 ms) were used to indicate pore-level growth behavior. After the hydrate formation ceased, dissociation was triggered by slowly reducing the pore pressure down to atmospheric pressure.

RESULTS AND DISCUSSION

Calibration Study
The correlation between average voxel intensity from MR imaging of the whole cores and the global water saturation is found to be linear (Figure 2). However, the intercept of the regression line with the y-axis is not at zero signal intensity meaning that a two-fold increase in the water saturation does not lead to a two-fold increase in the signal intensity. The average voxel intensity drops to zero at a water saturation of approximately 20%. Signal intensity calculations based on the specific RAREst protocol used in these experiments can thus not be used to infer the water saturation during

hydrate growth if the water saturation drops below 20%. Below this critical water saturation, the water will mostly be distributed as a thin film covering the water-wet grains and the T_2 decay will be too fast to be acquired with an echo time of 5.66 ms. The importance of the applied reference power is also demonstrated as decreasing the power results in higher signal intensity. The reference power is the peak power of a 1 ms 90° pulse and is calculated by the software at the start of each new study. However, cores with water saturation lower than ~40%, contains insufficient amounts of water for the reference power to be set automatically. The reference power must therefore manually be fixed to the same value as the software calculated for cores containing enough water. Figure 2 highlights the importance of keeping control of the reference power when comparing signal intensity acquired from different cores. The same applies for the receiver gain, which was held constant equal to 101 (dimensionless) during all scans.

Hydrate Study

A total of 42±3% of the pore space was filled with solid hydrate after the formation process had come to an end (S_w = 31% and S_g = 27%). The hydrate distribution was heterogeneous compared to the initial water saturation (Figure 3) indicating that the growth process took place at discrete locations in the core and that further spatial propagation of the hydrate growth was limited by mass transport. Formed hydrate layers acted as barriers between the water and gas phase and resulted in areas with substantial amounts of liquid water. The amplitude of the T_2* distribution decreased during hydrate growth in response to the conversion of liquid water to solid hydrate (Figure 4). T_2* is the measured time constant for the decay of transverse magnetization and is always less or equal to the true T_2 value. The decrease of the signal was largest for the highest T_2* values indicating pore-filling hydrate growth in the largest pores. The distribution also shifted leftwards during growth because the hydrate forming in the middle of pores led to an enhanced surface-to-volume ratio for the remaining liquid water [20].

Controlled pressure depletion of the core at constant volumetric rate led to signal reduction as water drained out from the core and into connected flow lines, primarily because of gas expansion. The water saturation continued to decrease until the pressure was lowered to approximately 6.0 MPa. At this point, the water saturation was low enough to become stagnant and gas could flow freely without displacing water. Some of the signal loss during the depressurization period may also be attributed to reformation of hydrates. Dissolved gas vaporization, gas expansion and two-phase flow induce many new interfacial contacts between water and gas and can thus trigger further hydrate growth during initial pressure drawdown [21- 22]. As the pressure was lowered below the hydrate stability pressure, the signal intensity increased again as the hydrate-encaged water was liberated to the liquid water phase. However, the final signal intensity was much lower than the initial intensity prior to hydrate formation because of water production into the connected flow line during pressure drawdown. This highlights the inherent problem of substantial water production when methane is recovered by hydrate dissociation.

CONCLUSIONS

Signal intensity quantification from high field MR imaging is correlated with known water saturation in Bentheimer sandstones. The relationship between signal intensity and water saturation is found to be linear, but a threshold saturation of 20% water is needed to provide measurable MR signal in this study. Hydrate formed from brine (0.1 wt% NaCl) and a gas mixture (22% propane and 78% methane) at P = 10.0 MPa and T = 21°C, is spatially visualized by the RAREst protocol. The final hydrate saturation of 42±3% is successfully estimated by signal intensity analysis. T_2 distributions obtained by CPMG scans during hydrate formation is used to infer pore-filling hydrate growth in these sandstones.

NOMENCLATURE

L – core length	[frac.]
P – pressure	[MPa]
$p\ (T_2^*)$ – relative amount of measured T_2^*	[-]
S_g – gas saturation	[%]
S_w – water saturation	[%]
T – temperature	[°C]
T_2 – natural time constant for decay of transverse magnetization	[s]
T_2^* – measured time constant for decay of transverse magnetization	[s]

ACKNOWLEDGEMENTS

The authors would like to acknowledge the Academia agreement between Equinor and the University of Bergen. One of the authors is indebted to the Research Council of Norway (grant number 255490).

REFERENCES

1. Sloan, E.D. and C.A. Koh, “Clathrate Hydrates of Natural Gases”. 3rd ed. CRC Press, Boca Raton, (2008).
2. Collett, T.S., R. Boswell, M.W. Lee, B.J. Anderson, K. Rose and K.A. Lewis, “Evaluation of Long-Term Gas-Hydrate-Production Testing Locations on the Alaska North Slope”. *SPE Res Eval & Eng*, (2012) **15**(2): p. 243 - 264.
3. Schoderbek, D., K.L. Martin, J.J. Howard, S. Silpngarmlert and K. Hester, “North Slope Hydrate Fieldtrial: CO2/CH4 Exchange”, in *Offshore Technology Conference*, (2012), Houston, USA.
4. Kawamoto, T., “The First Offshore MH Production Test”, (2013). Available from: http://energy.gov/sites/prod/files/2013/06/f1/Takami%20Kawamoto%20-%20The%20First%20Offshore%20Production%20Test.pdf. Accessed: January 6, 2014.
5. Kvamme, B., A. Graue, T. Buanes, T. Kuznetsova and G. Ersland, “Storage of CO2 in natural gas hydrate reservoirs and the effect of hydrate as an extra sealing in cold aquifers”. *International Journal of Greenhouse Gas Control*, (2007) **1**(2): p. 236-246.

6. Tohidi, B., J. Yang, M. Salehabadi, R. Anderson and A. Chapoy, "CO2 Hydrates Could Provide Secondary Safety Factor in Subsurface Sequestration of CO2". *Environmental Science & Technology*, (2010) **44**(4): p. 1509-1514.
7. Heindel, T.J., "A Review of X-Ray Flow Visualization With Applications to Multiphase Flows". *Journal of Fluids Engineering,* (2011) **133**(7): p. 1-16.
8. Kulenkampff', J., M. Grundig, M. Richter and F. Enzmann, "Evaluation of positron-emission-tomography for visualisation of migration processes in geomaterials". *Physics and Chemistry of the Earth*, (2008) **33**(14-16): p. 937-942.
9. Ersland, G., M.A. Fernø, A. Graue, B.A. Baldwin and J. Stevens, "Complementary imaging of oil recovery mechanisms in fractured reservoirs". *Chemical Engineering Journal*, (2010) **158**(1): p. 32-38.
10. Baldwin, B.A., A. Moradi-Araghi and J.C. Stevens, "Monitoring hydrate formation and dissociation in sandstone and bulk with magnetic resonance imaging". *Magnetic Resonance Imaging*, (2003) **21**(9): p. 1061-1069.
11. Graue, A., B. Kvamme, B.A. Baldwin, J. Stevens, J.J. Howard, E. Aspenes, G. Ersland, J. Husebø and D. Zornes, "MRI Visualization of Spontaneous Methane Production From Hydrates in Sandstone Core Plugs When Exposed to CO2". *SPE Journal*, (2006) **13**(2): p. 146-152.
12. Ersland, G., J. Husebø, A. Graue, B.A. Baldwin, J.J. Howard and J. Stevens, "Measuring gas hydrate formation and exchange with CO2 in Bentheim sandstone using MRI tomography". *Chemical Engineering Journal*, (2010) **158**(1): p. 25-31.
13. Hirai, S., Y. Tabe, K. Kuwano, K. Ogawa and K. Okazaki, "MRI Measurement of Hydrate Growth and an Application to Advanced CO2 Sequestration Technology". *Annals of the New York Academy of Sciences*, (2000) **912**(1): p. 246-253.
14. Gao, S., W. House and W.G. Chapman, "NMR/MRI Study of Clathrate Hydrate Mechanisms". *The Journal of Physical Chemistry B*, (2005) **109**(41): p. 19090-19093.
15. Yang, M., Y. Song, Y. Zhao, Y. Liu, L. Jiang and Q. Li, "MRI measurements of CO2 hydrate dissociation rate in a porous medium". *Magnetic Resonance Imaging*, (2011) **29**(7): p. 1007-1013.
16. Pohmann, R., O. Speck and K. Scheffler, "Signal-to-noise ratio and MR tissue parameters in human brain imaging at 3, 7, and 9.4 tesla using current receive coil arrays". *Magnetic Resonance in Medicine*, (2016) **75**(2): p. 801-809.
17. Niendorf, T., A. Pohlmann, H.M. Reimann, et al., "Advancing Cardiovascular, Neurovascular and Renal Magnetic Resonance Imaging in Small Rodents Using Cryogenic Radiofrequency Coil Technology". *Frontiers in Pharmacology*, (2015) **6**(255).
18. Öz, G., I. Tkáč and K. Uğurbil, "Animal models and high field imaging and spectroscopy". *Dialogues in Clinical Neuroscience*, (2013) **15**(3): p. 263-278.
19. Colorado School of Mines, Center for Hydrate Research, hydrate simulator *CSMgem*, (2015). Available from: http://hydrates.mines.edu/CHR/Software.html. Accessed: October 10, 2017.

20. Kleinberg, R.L., C. Flaum, D.D. Griffin, P.G. Brewer, G.E. Malby, E.T. Peltzer and J.P. Yesinowski, "Deep sea NMR: Methane hydrate growth habit in porous media and its relationship to hydraulic permeability, deposit accumulation, and submarine slope stability". *Journal of Geophysical Research: Solid Earth*, (2003) **108**(B10): p. 1-17.
21. Kneafsey, T.J., L. Tomutsa, G.J. Moridis, Y. Seol, B.M. Freifeld, C.E. Taylor and A. Gupta, "Methane hydrate formation and dissociation in a partially saturated core-scale sand sample". *Journal of Petroleum Science and Engineering*, (2007) **56**(1-3): p. 108-126.
22. Xiong, L., X. Li, Y. Wang and C. Xu, "Experimental Study on Methane Hydrate Dissociation by Depressurization in Porous Sediments". *Energies*, (2012) **5**(2): p. 518-530.

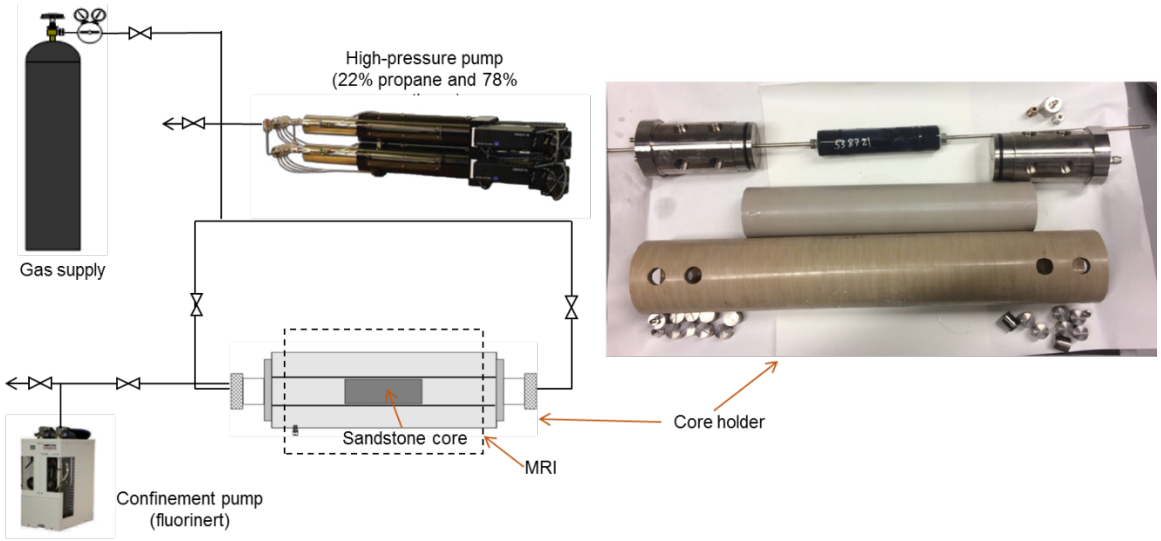

Figure 1. Schematic of experimental setup with close-up of disassembled core holder to the right. The core is placed inside the rubber sleeve with end-pieces and connected flow lines mounted on each side. The confinement fluid will surround the sleeve and be kept in place by the liner.

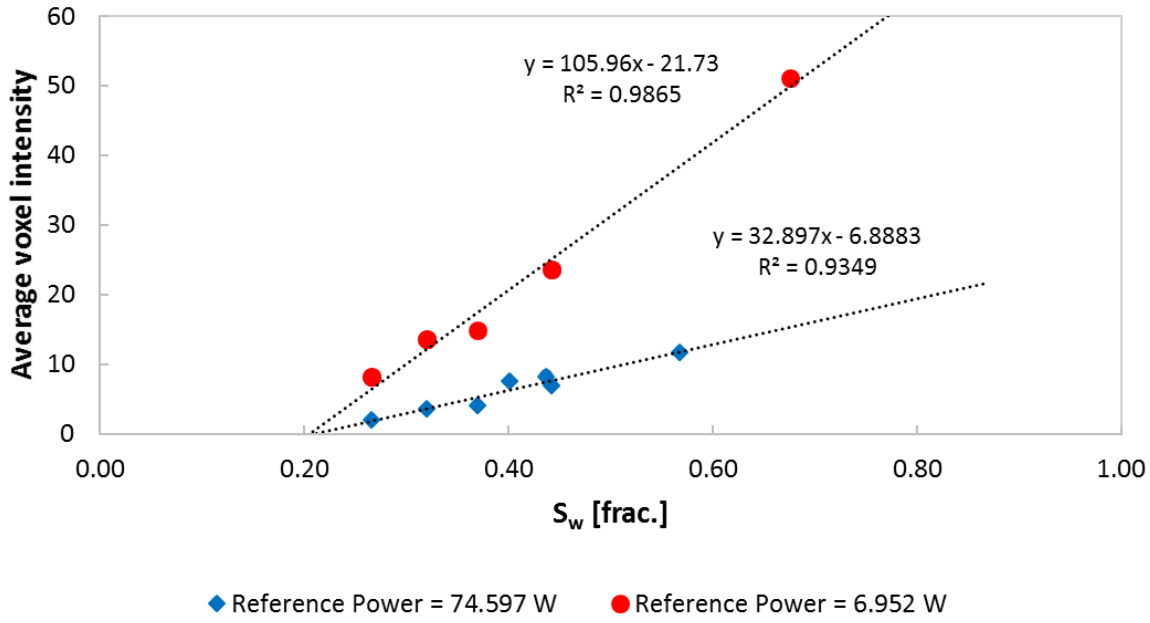

Figure 2. Correlation between average voxel intensity from MR imaging and water saturation. Each data point on the plot corresponds to average water saturation and average voxel intensity for an individual Bentheimer sandstone. Notice that the relationship between intensity and saturation is linear, but depends strongly on the applied reference power for high field MRI.

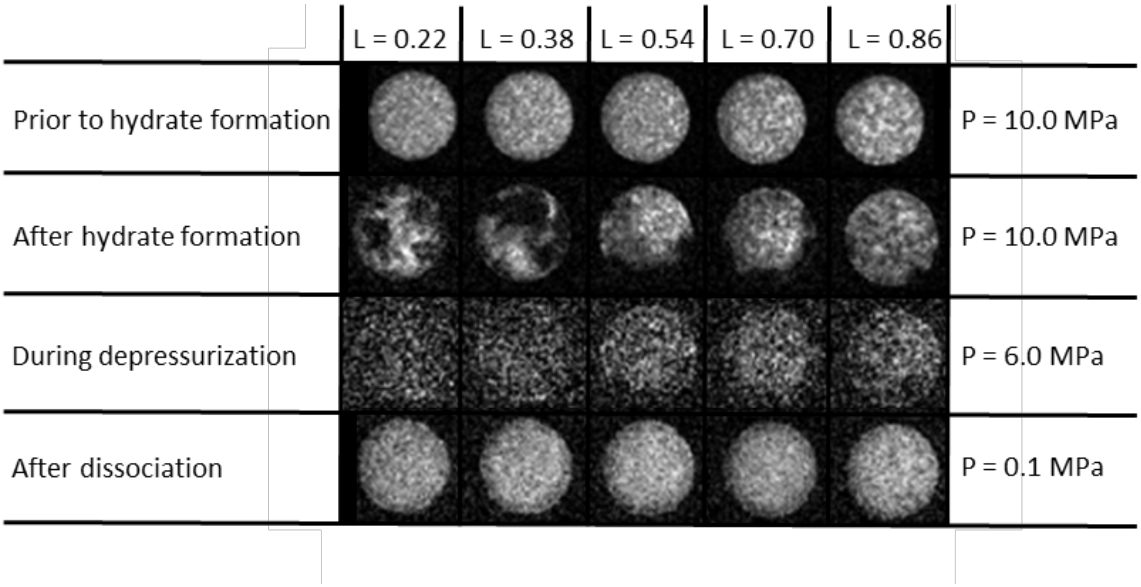

Figure 3. Cross-sectional MR images of hydrate formation and dissociation at room temperature (21°C). Grey-scale intensity relates to water saturation. The core is saturated with 65% water and 25% gas (22% propane and 78% methane) prior to hydrate formation. The hydrate growth is heterogeneous throughout the length of the core and a final hydrate saturation of 42±3% is reached. Water is produced out from the core during depressurization and leads to a decrease in signal intensity. A homogenous water saturation is reestablished after all the hydrates have melted.

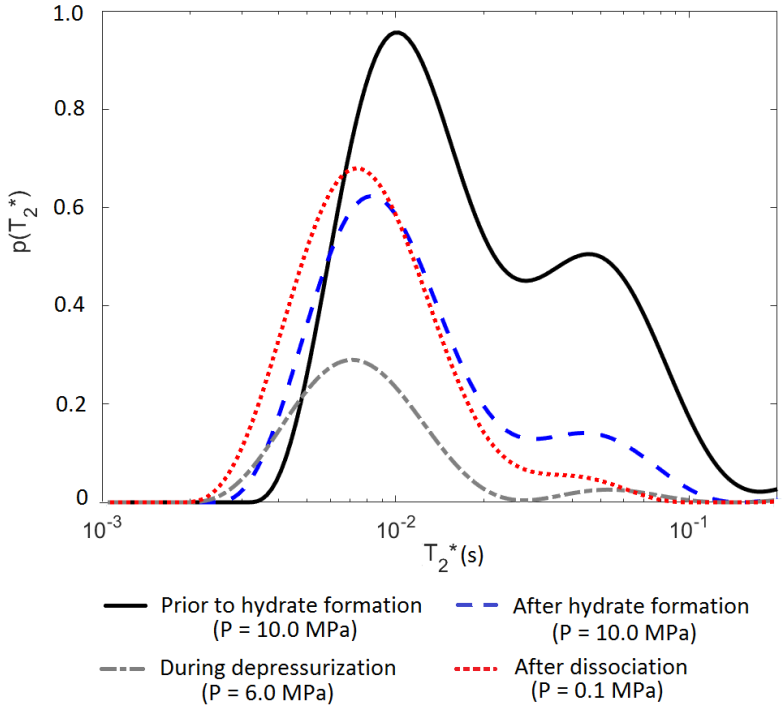

Figure 4. T2* distribution curves of hydrate formation and dissociation at room temperature (21°C). Y-axis denotes normalized amount of given T2* value. The magnitude of the distribution decreases during growth corresponding to loss of signal as liquid water is converted to solid hydrates. The amplitude decreases further during depressurization as water is expelled out from the core. Melting the hydrates completely leads to reemergence of the signal.